

A PARAMETRIC STUDY OF THE DEPLOYABLE WING AIRPLANE FOR MARS EXPLORATION

Koji Fujita*

*** Department of Aerospace Engineering, Tohoku University, Sendai, Japan
6-6-01, Aramaki-Aza-Aoba, Aoba-ku, Sendai, Miyagi 980-8579, Japan**

Tel. & Fax: +81-22-795-4075

fujita.koji@aero.mech.tohoku.ac.jp

Keywords: UAV, Low Reynolds number, Wing and tail deployment, Parametric study, Propeller

Abstract

A deployable airplane for Mars exploration offers the possibility to obtain high-resolution data over a wide range. This paper presents a conceptual design method for the deployable airplane for Mars. A parametric study was conducted to improve the performance. Feasible specifications of a deployable airplane are proposed as a result of the constructed method. The total mass and range of the proposed airplane are 7.8 kg and 54 km, respectively. Finally, effectiveness of future technology developments is quantitatively clarified to provide a guideline for development.

1 Introduction

Application of airplanes for Mars exploration has seriously considered as a new effective exploration method [1]. Airplanes can fly over a wide range, which is impossible for rovers. In addition, the airplane also can obtain higher resolution data than satellites because its flight altitude is one-hundredth of that of the satellites. Therefore, the use of airplanes for Mars exploration will bring novel scientific efforts.

Previously Fujita et al. developed a basis of the conceptual design method for deployable airplane on Mars and proposed one of the feasible designs [2]. However the design was not optimal and had a possibility of the improvement. In addition, effect of the input parameter change on the airplane performance has not been clarified yet. Knowledge of this effect is important to improve design and to

conduct technology developments for the airplane. Furthermore, some of the design parameter should be update.

This paper presents an updated conceptual design method, parametric study results, a design proposal of the deployable airplane for Mars, and effectiveness of the future technology development.

2 Conceptual Design Method

A conceptual design process basically followed “*Aircraft Design: A Conceptual Approach*” by Raymer [3]. First, the design requirements and constraints were defined. Next, a first guess on sizing was made from a sketch. Then, the values about aerodynamics, weight, propulsion system, etc. were estimated. Finally, the design was revised based on that result and sizing was made again. Through iterating this cycle, the design was optimized and detailed. In consideration of the low Reynolds number flow, this study uses results of aerodynamic characteristics experiments at low Reynolds number [4, 5].

A mission scenario had been defined in the previous paper [6]. The Mars airplane will be transported to Mars packed in an aeroshell. At Mars, the aeroshell will enter and descend into Martian atmosphere. When the aeroshell arrives at a predefined position, the Mars airplane will be released from the aeroshell. Then it will deploy, control its attitude, and start horizontal flight. It will observe a Martian magnetic field and take pictures of a Martian surface.

Table 2.1 presents requirements and constraints assumed on the basis of the mission

scenario and available experimental data. These were used in estimation method as inputs.

Table 2.1. Requirements and Constraints.

Item	Value / Comment
Equipment mass (w/o battery)	3.0 kg
Equipment power	54 W
Maximum aspect ratio	8 -
Minimum aspect ratio	4 -
Maximum main wing Mach #	0.3 -
Maximum propeller Mach #	0.7 -
Aeroshell diameter	1.0 m
Aeroshell length	0.6 m
Configuration	Fixed wing
Propulsion	Propeller / DC motor
Payloads	Magnetometer High-resolution camera

A flow chart of the specification estimation method is shown in Fig. 2.1. The specifications of the Mars airplane were estimated through iterations. This method was made up of five sections: aerodynamic performance and geometry estimation, propulsion performance estimation, power consumption estimation, basic mass estimation, and deployment mechanism mass estimation.

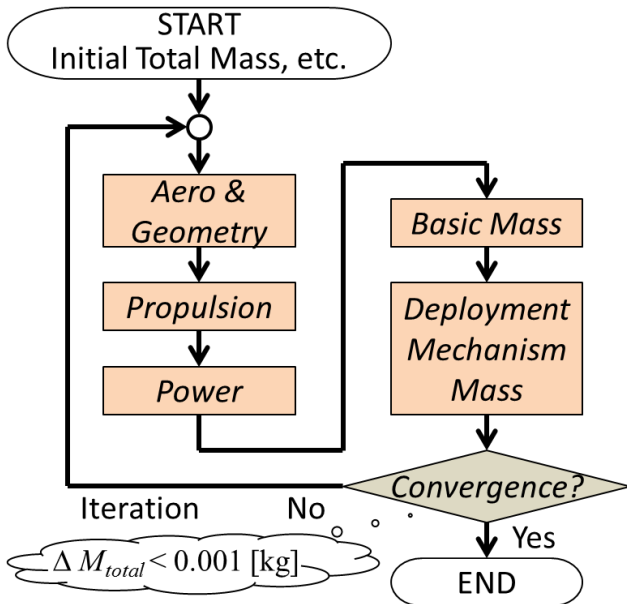


Fig. 2.1. The Flow Chart of the Specification Estimation Method.

In order to reduce energy consumption for the propulsion system, the Mars airplane was designed to maximize a lift-drag ratio during non-accelerated level flight while satisfying

requirements and constraints. A main wing area S_{ref} was given using Eq. (1).

$$S_{ref} = \frac{2M_{total}g}{\rho V^2 C_L}. \quad (1)$$

At first, total mass M_{total} was assumed to be 8 kg as an initial value. The acceleration due to gravity g was set to 3.7 m/s^2 . Cruise velocity V was input parameter. Density ρ was given from flight altitude. A lift coefficient of the main wing C_L was calculated using Eqs. (2) and (3). These equations were based on the previous paper [7] and a little modified.

$$Re < 2.1 \times 10^4 \\ C_L = 1.7 \times 10^{-5} \times Re + 0.012AR + 0.084. \quad (2)$$

$$Re \geq 2.1 \times 10^4 \\ C_L = -0.031 \ln(Re - 2.0 \times 10^4) \\ + 0.0080AR + 0.69. \quad (3)$$

A main wing span was given as an input parameter. Chord length and aspect ratio were obtained using wing area and span.

Horizontal and vertical areas were obtained using tail volume coefficients. Horizontal and vertical tail volume coefficients were set to 0.5 and 0.04 respectively as a typical value [3]. Aspect ratio was given as an input parameter. Span and chord length were obtained using tail area and aspect ratio.

Required diameter of a tail boom $d_{TailBoom}$ was obtained using following equations:

$$d_{TailBoom} = \max(d_1, d_2), \quad (4)$$

$$d_1 = \sqrt[3]{\frac{4Pl^2}{\pi E \theta t}}, \quad (5)$$

$$d_2 = \sqrt[3]{\frac{4Tl \times 2(1+\nu)}{\pi E \phi t}}, \quad (6)$$

where d_1 and d_2 are required diameters for bending and torsion, respectively. θ and ϕ are allowable angle of deflection and torsion, respectively. Both values were set to 0.5 degrees. The equations assumes thin cylinder. Thickness t was set to 0.6 mm. l is a tail boom length.

Material was set to isotropic carbon fiber reinforced plastic (CFRP). Young's modulus E was set to 300 GPa [8]. Poisson ratio ν was assumed to be 0.3. Bending load P and torsional moment T were estimated as follows:

$$P = qS_{HT}C_{L,T,max} , \quad (7)$$

$$T = \frac{b_{VT}}{2} qS_{VT}C_{L,T,max} , \quad (8)$$

where q , b_{VT} , S_{HT} , and S_{VT} are dynamic pressure, vertical tail span, horizontal and vertical tail area, respectively. Maximum lift coefficient of the tail $C_{L,T,max}$ was assumed to be 1.

Then a drag was estimated. The estimation process basically followed previous paper [2]. A drag coefficient of the main wing was based on the previous paper [7] and modified due to minimum drag correction. Equation (9) shows the drag coefficient of the main wing C_{Dw} formulated as a function of Reynolds number Re and aspect ratio AR .

$$C_{Dw} = 0.78Re^{-0.28} - 0.0022AR - 0.015 . \quad (9)$$

A drag coefficient of the tail wing was assumed to be a zero-lift drag coefficient and corrected using ratio of the main wing and tail areas. The drag coefficient of the fuselage C_{Df} was represented as the following equation [3]:

$$D_{Df} = \frac{1.328}{\sqrt{Re_l}} \left(1 + \frac{60}{f^3} + \frac{f}{400} \right) \frac{S_{f,wet}}{S_{ref}} , \quad (10)$$

where Re_l is Reynolds number by fuselage length, f is a fuselage taper ratio, and $S_{f,wet}$ is wetted area of the fuselage. A drag coefficient of the tail boom was also estimated like fuselage. The total drag coefficient was obtained as the sum of those drag coefficients. The drag during cruising was then obtained.

A propulsion performance was estimated in accordance with a method developed by Adkins and Liebeck [9]. Here, results of the aerodynamic characteristics experiment at low Reynolds number were used [5, 7].

As a power consumption estimation, endurance and range were estimated using the following equations:

$$Endurance = \frac{M_{battery}\rho_{energy}}{P_{total}} , \quad (11)$$

$$Range = Endurance \cdot V , \quad (12)$$

where a battery mass $M_{battery}$ and energy density of the battery ρ_{energy} were set to 0.2 kg and 116 Wh/kg, respectively. A total power P_{total} was calculated as a sum of the power of the motor and the equipment. The power of the equipment was set to 54 W, based on a preliminary thermal analysis [10].

A total mass was estimated as a sum of a mass of each section. The main wing and tail mass were estimated using wing areal density, 0.4 kg/m² [11]. The fuselage skin was made by CFRP, and its density was 1800 kg/m³. A fuselage floor board was installed inside the fuselage. Its length was same to the fuselage skin and the width was 40 % of the fuselage diameter and the thickness was 2 mm. Its density was set to 290 kg/m³. A material of the propeller blade was CFRP. The blade geometry was designed using Adkins and Liebeck's method [9]. A mass of the motor was obtained as a function of the torque [2]. A mass of a speed controller was set to 0.17 kg. Onboard equipment included avionics, power system, communication system, air data sensor system, payload, and margin. A mass of the equipment without the battery was set to 3.0 kg, including 0.3 kg of the margin mass.

Next, deployment mechanisms mass was estimated. A folding method was adopted as a deployment mechanism. Spring hinges were used as a deployment actuator. An estimation method for wing deployment mechanism mass was reported in the previous paper [2]. This method considered maximum hinge torque due to aerodynamic force. The spring hinge mass M_{sh} was estimated from empirical formula using the maximum hinge torque T_{hinge} .

$$M_{sh} [g] = 33.6 \times T_{hinge} [N \cdot m] + 5.65 . \quad (13)$$

In addition to the previous paper, this paper adopted a similar method to the tail deployment mechanism mass estimation. It is more complicated than main wing to design tail deployment mechanism. The main wing can be

folded anywhere on the wing. However tail side can be folded only on the tail boom and cannot be folded on the tail due to the existence of the vertical tail. Figure 2.2 illustrates the hinge position. Here, a , c , and D_{shell} are the length between the hinge and leading edge of the tail, the tail chord length, and the aeroshell diameter, respectively. A clearance ratio r was set to 0.9. When the predicted hinge line (red-dot line in Fig. 2.2.) lied on the tail, the hinge line position was moved to the leading edge of the tail, as shown in Fig. 2.2. This change is possible when

$$c \leq a. \quad (14)$$

Hence the tail chord length was restricted. This limitation is not suitable for conceptual design because the limitation changes depending on the tail position. Therefore in this paper, the tail chord length was limited as follows:

$$c \leq \frac{rD_{shell}}{2}. \quad (15)$$

Under this limitation, the hinge can lie on the tail leading edge regardless of the tail position.

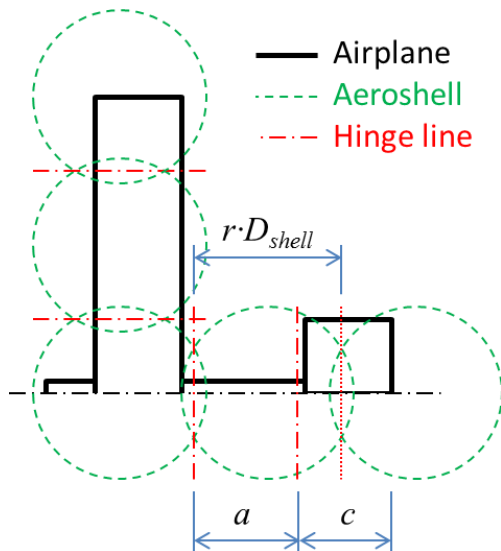


Fig. 2.2. The Schematic Illustration of the Hinge Position.

By reentering the obtained total mass to Eq. (1), calculations were iterated until a difference of the total mass became less than 0.001 kg.

A nose position was set to 0.05 m inside from an aeroshell edge. A length between the fuselage and the main wing was defined where

the center of gravity of the airplane lied on the specified point. The center of gravity position was set to 30 % of the main wing chord.

3 Analysis Method

The conceptual design method was analyzed through following three steps:

1. Design method improvement
2. Trade-off study
3. Evaluation for technology development

Firstly, the design method was improved. Here, parametric study was conducted to clarify a relation between input parameters and objective functions. Then some input parameters were maximized or minimized. Secondly, a trade-off study was performed to reveal Pareto design solutions. Finally, effectiveness of future technology developments was evaluated to provide a guideline for development. Objective functions in this paper were set to a total mass and range.

3.1 Design Method Improvement

Input parameters can be categorized into two types. One is technical constants such as energy density of a battery, wing areal density, aerodynamic characteristics, and so on. It is impossible for designer to change these values freely. Another is design parameters such as cruise velocity, tail moment arm, propeller diameter, and so on. These parameters can be changed freely.

A goal of this step is to search the input design parameters which should be maximized or minimized and to reflect it to the conceptual design method. Currently there are eight input design parameters as shown in Table 3.1. However, some of the input design parameters should not be designed freely and they should be maximized or minimized. Parametric studies for input design parameters were performed to determine if the input design parameter should be maximized (minimized) or has a trade-off relation for objective functions. Then the parameter which should be maximized (minimized) were fixed to the maximum

(minimum) value and removed from input parameters list. Only the parameters which have a trade-off relation remained as input parameters through iterating this step.

Table 3.1 Input Design Parameters in the Initial Conceptual Design Method

Cruise velocity	Horizontal tail aspect ratio
Main wing span	Propeller diameter
Battery mass	Propeller root diameter
Tail moment arm	Propeller rotation speed

3.2 Trade-off Study

Trade-off study was performed for the remaining input design parameters to clarify Pareto design solutions. Then one of the Pareto design was proposed.

3.3 Evaluation for Technology Development

The current conceptual design method is based on currently available technologies. These technologies may improve through future development. Here, these values were parametrically changed to 50 % or 150 % and these impacts to the design were revealed. Evaluated parameters are shown in Table 3.2.

Table 3.2 Evaluated Parameters.

Parameters	Value [Unit]
Mass of deployment mechanisms	- [kg]
Mass of equipment (without a battery)	3.0 [kg]
Power of equipment	54 [W]
Power of a motor	- [W]
Energy density of a battery	116 [Wh/kg]
Drag	- [N]
Fuselage diameter	0.14 [m]
Fuselage length	0.6 [m]
Wing areal density	0.4 [kg/m ²]
Maximum main wing Mach number	0.3 [-]

4 Results and Discussion

4.1 Design Method Improvement

4.1.1 Initial Design

Figure 4.1 illustrates plane view of an initial design. Figure 4.2 shows its mass breakdown. Table 4.1 lists specifications of the initial design. The initial design is low performance. Total mass was 7.2 kg and range was only 23 km.

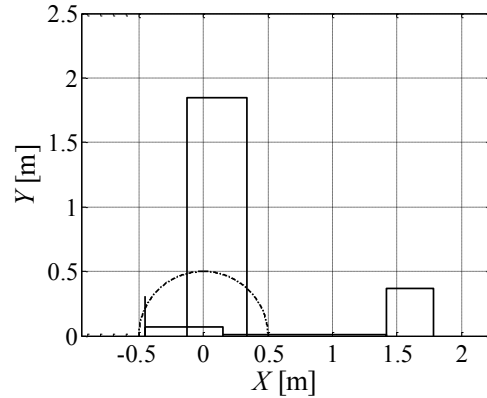


Fig. 4.1. The Plane View of the Initial Design.

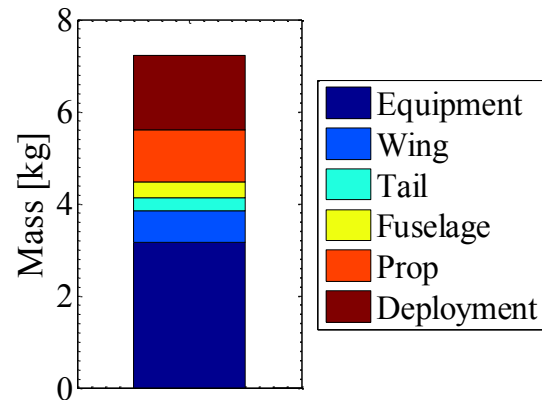


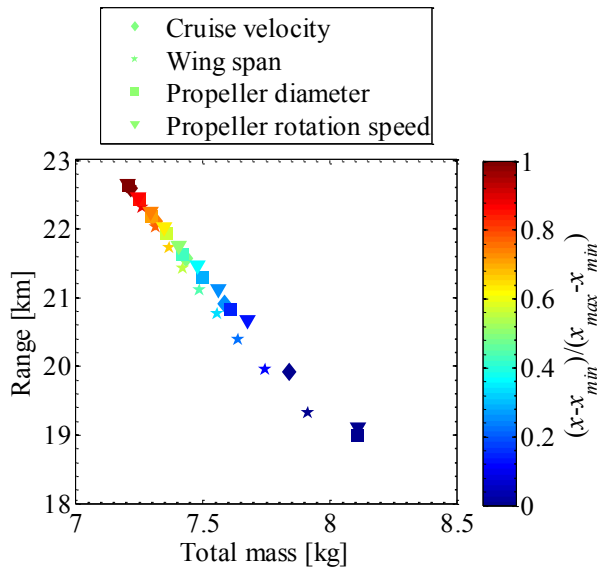
Fig. 4.2. The Mass Breakdown of the Initial Design.

Table 4.1. The Specifications the Initial Design.

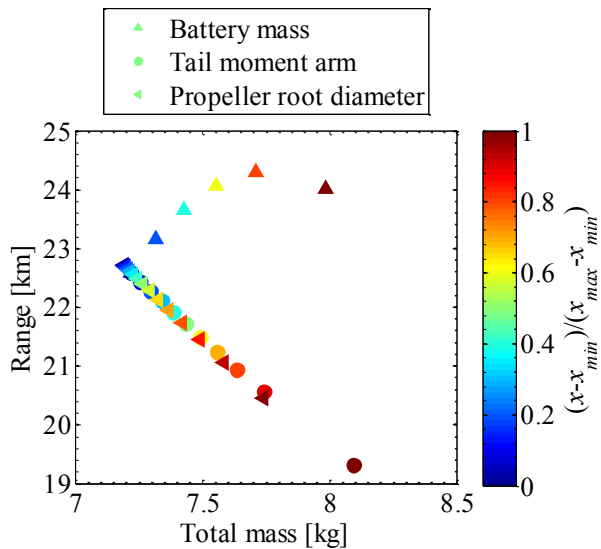
Parameters	Value	Unit
Span	3.7	m
Chord	0.47	m
Cruise velocity	68	m/s
<i>Re</i> number (main wing)	3.9	10 ⁴
<i>M</i> number (main wing)	0.28	-
Drag	1.62	N
Lift-to-drag ratio	16.5	-
Propeller diameter	0.62	m
Propeller rotation speed	4500	rpm
Motor power	196	W
Battery mass	0.2	kg
Total mass	7.2	kg
Range	23	km
Endurance	6	min

4.1.2 First Iteration

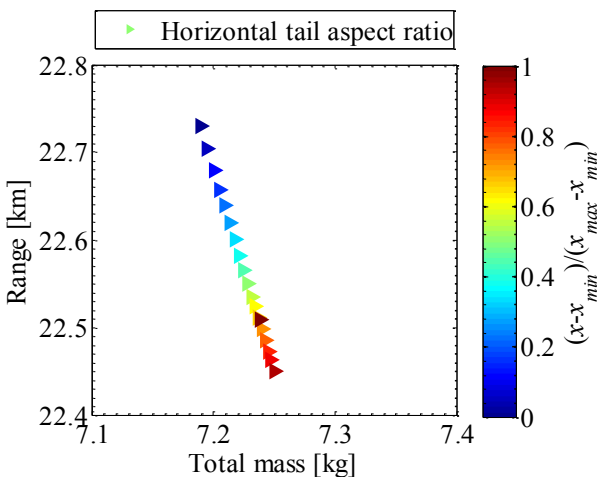
Figure 4.3 shows a parametric study result at the first iteration. *X* and *Y* axes are total mass and range, respectively. Therefore a design plotted at left upper side is better solution. Table 4.2 provides tendency and limit. A battery mass naturally shows the trade-off relation. Many other parameters are restricted by the main wing aspect ratio. This is the limitation of the available aerodynamic characteristics data.



a. Cruise Velocity, Wing Span, Propeller Diameter, and Propeller Rotation Speed.



b. Battery Mass, Tail Moment Arm, and Propeller Root Diameter.



c. Horizontal Tail Aspect Ratio.

Fig. 4.3. The Parametric Study Result at First Iteration.

Table 4.2. Tendency and Limit at First Iteration.

Parameters	Tendency	Limit
Cruise velocity	More is better	Main wing aspect ratio (High)
Main wing span	More is better	Main wing aspect ratio (High)
Battery mass	Trade-off	-
Tail moment arm	Less is better	Main wing aspect ratio (High)
Horizontal tail aspect ratio	Less is better	Main wing aspect ratio (High)
Propeller diameter	More is better	Main wing aspect ratio (High)
Propeller root diameter	Less is better	Propeller strength
Propeller rotation speed	More is better	Main wing aspect ratio (High)

4.1.3 Second Iteration

A result of the first iteration indicates that high aspect ratio of the main wing brings better solution. Therefore the conceptual design method was changed as follows:

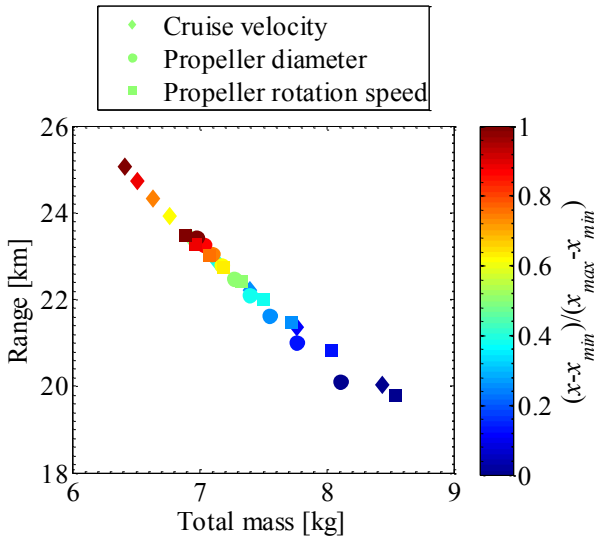
- Aspect ratio of the main wing became input parameter. The value was set to maximum.
- Span of the main wing became calculated parameter.

Here, propeller root diameter was set to adequate small value and not optimized because effect to the objective functions is small and the relation between propeller root diameter and required propeller strength is not explicit.

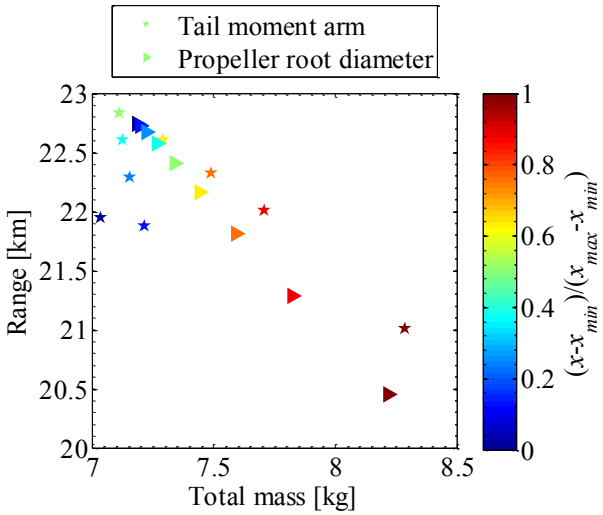
Figure 4.4 shows a parametric study result at the second iteration. Table 4.3 provides tendency and limit. The cruise velocity is restricted by the main wing Mach number. The tail moment arm shows trade-off relation. Figure 4.4.b shows zigzag line. It is caused by the change of the number of the tail hinges.

Table 4.3. Tendency and Limit at Second Iteration.

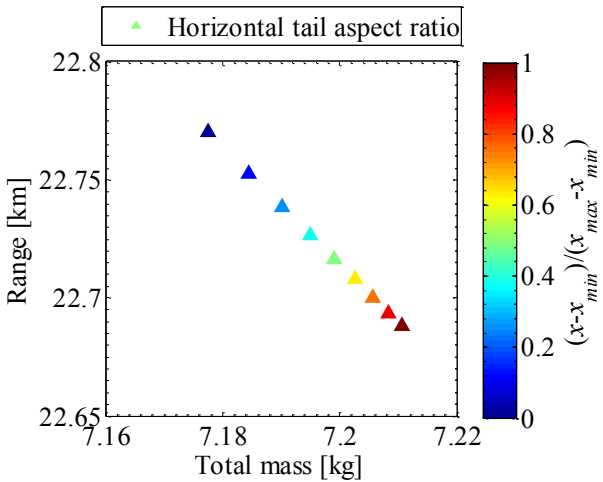
Parameters	Tendency	Limit
Cruise velocity	More is better	Main wing Mach number
Tail moment arm	Trade-off	-
Horizontal tail aspect ratio	Less is better	Horizontal tail chord
Propeller diameter	More is better	Propeller Mach number
Propeller root diameter	Less is better	Propeller strength
Propeller rotation speed	More is better	Propeller Mach number



a. Cruise Velocity, Propeller Diameter, and Propeller Rotation Speed.



b. Tail Moment Arm and Propeller Root Diameter.



c. Horizontal Tail Aspect Ratio.

Fig. 4.4. The Parametric Study Result at Second Iteration.

The propeller diameter and the propeller rotation speed are restricted by the propeller Mach number.

4.1.4 Third Iteration

A result of the second iteration indicated that high Mach numbers of the wing and propeller brought better solution. Hence the conceptual design method was changed as follows:

- Main wing Mach number became input parameter. The value was set to maximum.
- Propeller Mach number became input parameter. The value was set to maximum.
- Cruise velocity became calculated parameter.
- Propeller rotation speed became calculated parameter.
- Horizontal and vertical tail aspect ratio became input parameter. The values were set to minimum [3].
- Horizontal and vertical tail span became calculated parameter. When the tail chord reaches the aeroshell, the tail chord is restricted and aspect ratio becomes higher.

Through this change, only the propeller diameter remained as an analysis parameter. Because the analysis result shows trade-off relation, it will be discussed in the section 4.2.

Before the design method improvement, there were eight input design parameters. However, three parameters were remained as a trade-off parameter and other five parameters are optimized through the design method improvement process.

4.2 Trade-off Study

The remaining input design parameters (i.e. battery mass, propeller diameter, and tail moment arm) have a trade-off relation. Figure 4.5 shows result of the trade-off study for the parameters.

The battery mass had a huge effect on objective functions because the battery mass was directly concerned with the calculation of the objective functions as shown in Eq. (12).

On the other hand, though the relation was trade-off, the propeller diameter and the tail moment arm had a small effect. In addition, the

input range for Pareto solution was narrow. Hence these parameters should not be treated as trade-off parameters and should be designed at adequate point, neither maximum nor minimum.

A conceptual design was proposed using the result of the trade-off study. Proposed design was about a middle point of the Pareto solution. Figure 4.6 illustrates the plane view of the proposed design baseline. Table 4.4 lists specifications of the proposed design. Figure 4.7 shows 3-D view of the proposed design.

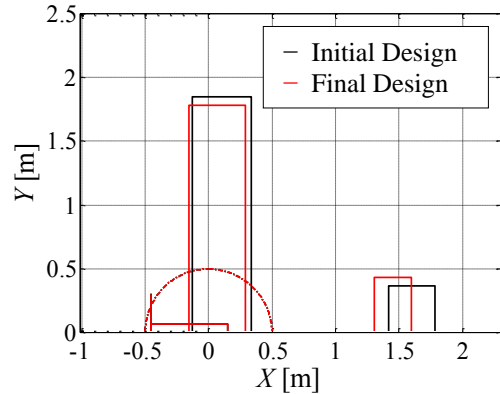


Fig. 4.6. The Plane View of the Proposed Design Baseline.

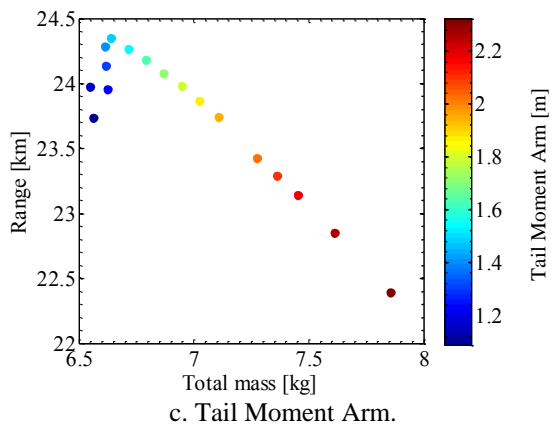
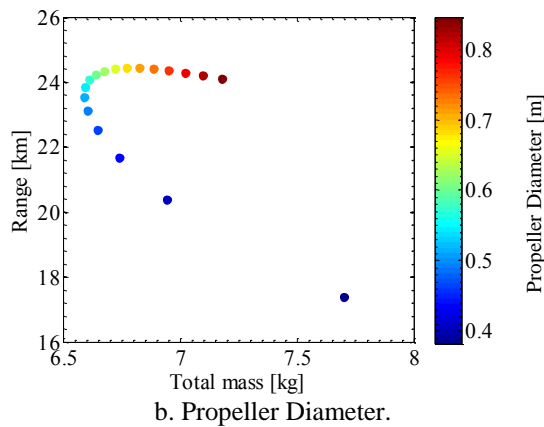
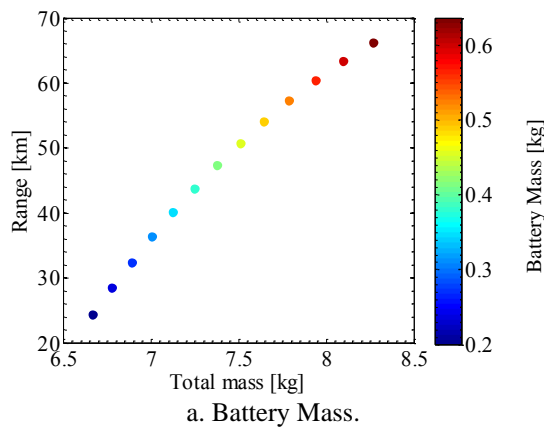


Fig. 4.5 Trade-off Study.

Table 4.4. The Specifications of the Proposed Design.

Parameters	Value	Unit
Span	3.6	m
Mean Aerodynamic Chord	0.48	m
Cruise velocity	73	m/s
Re number (main wing)	4.2	10^4
M number (main wing)	0.3	-
Drag	1.71	N
Lift-to-drag ratio	16.9	-
Propeller diameter	0.60	m
Propeller rotation speed	4277	rpm
Motor power	225	W
Battery mass	0.5	kg
Total mass	7.8	kg
Range	54	km
Endurance	12	min

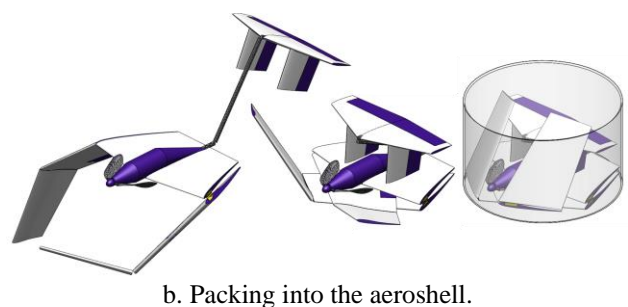
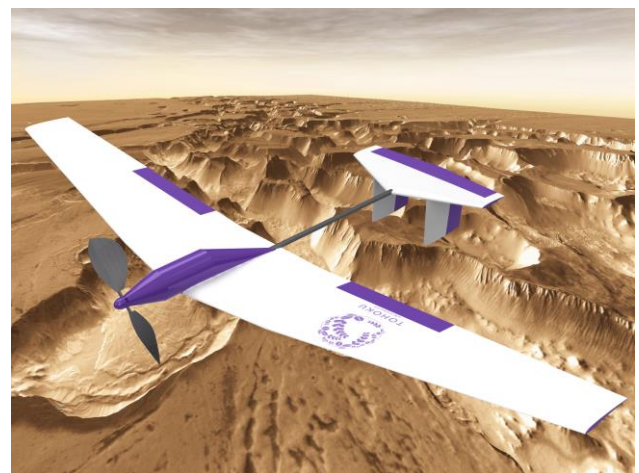


Fig. 4.7. The 3-D View of the Proposed Design.

4.3 Evaluation for Technology Development

Figure 4.8 shows a result of the parametric study of the future technologies. Figure 4.8.a. and 4.8.b. are the results of high and low impact parameters, respectively.

As shown in Fig. 4.8.a., a reduction of the deployment mechanism mass and the equipment mass achieved not only the total mass reduction but also range increase. This range increase is due to the drag reduction through downsizing. On the other hand, an increase of the battery energy density and a decrease of the motor power achieved a range increase. This range increase is due to endurance increase. A reduction of the drag achieved a total mass reduction and a range increase. The total mass reduction is mainly due to the propulsion system mass reduction. The range increase is due to the reduction of the motor power.

As shown in Fig. 4.8.b., the fuselage length and the main wing Mach number shows interesting tendency. As the fuselage length shortened, the total mass reduced at first. This is due to the reduction of the fuselage structural mass. However, as the fuselage length became shorter enough, the total mass increased and the range shortened. This is due to the drag increase. Figure 4.9 presents the total and fuselage drag coefficient vs. change ratio of the fuselage length. The fuselage drag coefficient increased and its increment is about 10 % of the total drag coefficient. This drag increase causes increase of the propulsion system mass, as shown in Fig. 4.10. On the other hand, optimal wing Mach number was about 1.3 times higher than current design, as shown in Fig. 4.8.b. Figure 4.11 shows the mass breakdown vs. change ratio of the main wing Mach number. As the Mach number increased, the total mass reduced at first. This is mainly due to the reduction of the required wing area. However, as the Mach number became higher enough, the total mass increased. This is due to the increase of the propulsion system mass.

As mentioned above, the effect of the future technology development on the deployable airplane for Mars exploration was quantitatively revealed. The performance improvement is expected through a combination

of those developments. Note that it is still not clear that which technology development should be focused on because a possibility of the development is different each other.

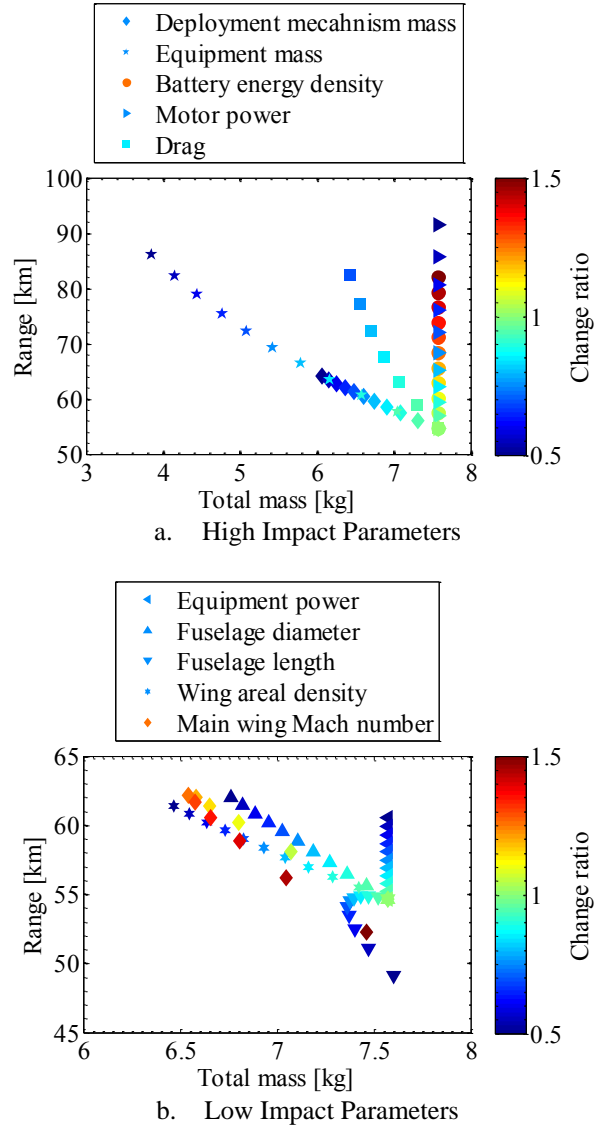


Fig. 4.8. The Parametric Study of the Future Technologies.

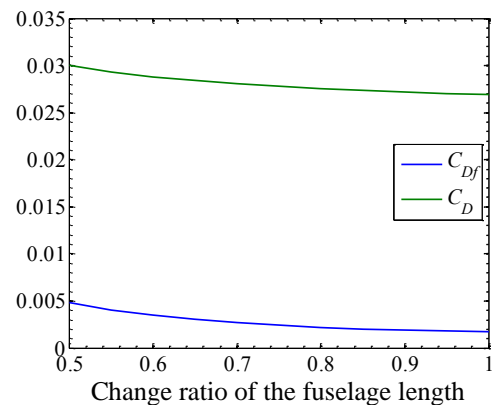


Fig. 4.9. The Total and Fuselage Drag Coefficients vs. Change Ratio of the Fuselage Length.

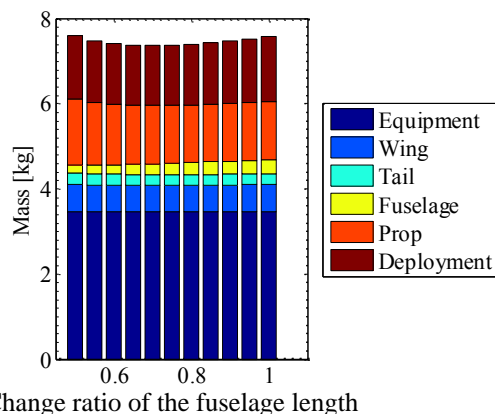


Fig. 4.10. The Mass Breakdown vs. Change Ratio of the Fuselage Length.

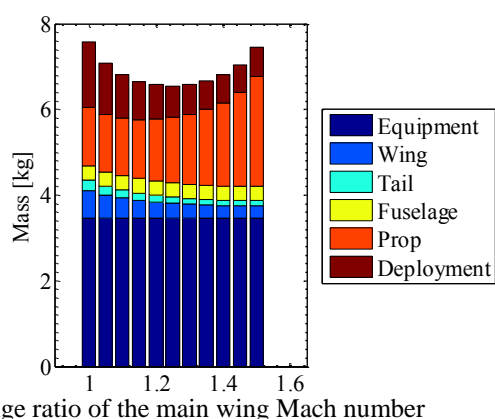


Fig. 4.11. The Mass Breakdown vs. Change Ratio of the Main Wing Mach Number.

5 Conclusions

A conceptual design method of the deployable airplane for Mars exploration was constructed. A parametric study was performed and output design tendencies for each input parameter change were clarified. The battery mass showed trade-off relation between the total mass and range. The propeller diameter and the tail moment arm had adequate values. Other input design parameters examined in this paper should have been chosen maximum or minimum value. The conceptual design method was improved using this knowledge. The deployable airplane for Mars was proposed and this range is more than twice to the initial design. Finally the effect of the technology development on the deployable airplane for Mars exploration was quantitatively revealed.

Future works include analysis of the effect of the aeroshell size and design case study. It is also required to clarify the relation among

mission payload, required range, minimum aeroshell size, and airplane design.

References

- [1] Kubota T. Japan's Mars Exploration Plan. *Proc. of the 2nd Annu. Symp. on Planetary Exploration*, 2010.
- [2] Fujita K, et al. Conceptual Design with Aerial Deployment Mechanisms of Airplane for Mars. *Proc. of the 2012 Asia-Pacific Int. Symp. on Aerospace Tech.*, #1.7.4. Jeju, Korea, Nov, 2012.
- [3] Raymer D. P. *Aircraft Design: A Conceptual Approach*, AIAA Education Series.
- [4] Shigeoka S, et al. Variable-pressure Wind Tunnel Study of Aspect Ratio Effects on Three-Dimensional Wing at Low Reynolds Number Flow. *Proc. of the 64th Kyushu Branch Regular Meeting of the JSME*, C42, Kyushu University, Fukuoka, Japan, 2011.
- [5] Suwa T, et al. Aerodynamic Characteristics of a Triangular Airfoil at Low Reynolds Number and High-Subsonic Mach Number. *Proc. of the 43rd Fluid Dynamics Conf.*, 2011, 1D09, Tokyo, 2011.
- [6] Fujita K, et al. Conceptual Design of a Miniature, Propeller-Driven Airplane for Mars. *Proc. of the 50th AIAA ASM*, AIAA 2012-0847, Nashville, USA, 2012.
- [7] Fujita K, et al. Conceptual design method for a Mars airplane: Formulation of aerodynamic characteristics at low Reynolds numbers. *Proc. of the 9th Int. Conf. on Fluid Dynamics*, OS11-8, Sendai, Japan, 2012.
- [8] TORAY, TORAYCA prepreg 2255S-25, URL: <http://www.torayca.com/download/pdf/prepreg.pdf> [cited 25 June 2014].
- [9] Adkins C N and Liebeck R H. Design of Optimum Propellers. *Proc. of the AIAA 21st Aerospace Science Meeting*, AIAA-83-0190, Reno, USA, 1983.
- [10] Daimaru T, et al. Preliminary Design and Thermal Analysis of a Miniature Mars Airplane Thermal Control System. *Proc. of 43rd Int. Conf. on Environmental Systems*, AIAA 2013-3349, Vail, CO, USA, July, 2013.
- [11] Takeuchi S, et al. Conceptual Structure Design of Mars Exploration Aircraft. *Proc. of the 49th aircraft symp*, JSASS-2011-5228, Japan, Oct, 2011.

Copyright Statement

The authors confirm that they, and/or their company or organization, hold copyright on all of the original material included in this paper. The authors also confirm that they have obtained permission, from the copyright holder of any third party material included in this paper, to publish it as part of their paper. The authors confirm that they give permission, or have obtained permission from the copyright holder of this paper, for the publication and distribution of this paper as part of the ICAS 2014 proceedings or as individual off-prints from the proceedings.